ULTRA-WIDEBAND METAMATERIAL FILTER BASED ON ELECTROINDUCTIVE-WAVE COUPLING BETWEEN MICROSTRIPS

M. Navarro-Cía, J. M. Carrasco, M. Beruete, and F. Falcone

Millimeter and Terahertz Waves Laboratory
Universidad Pública de Navarra
Campus Arrosadía, Pamplona 31006, Spain

Abstract—In this work, we analyse the frequency response of microstrip lines coupled by complementary split ring resonators (CSRRs) etched on the ground plane supporting electroinductive waves (EIWs). The single-particle configurations demonstrate the principle of operation whose bandwidths reach 67% of the central frequency. A double configuration is afterwards investigated as a further improvement of the filtering response, such as the level of the spurious lower frequency band. Finally, an ultimate prototype comprising different CSRRs along the access line, together with the aforementioned EIW-coupling is proposed for filtering undesired higher bands. Experimental results confirm numerical analysis.

1. INTRODUCTION

The design of microwave planar filters and couplers has taken a great advantage of the new perspective brought along by the advent of metamaterials [1]. In particular, Split Ring Resonators (SRRs) [2] and CSRRs [3] have become powerful elements in planar technology as a result of their tailored frequency response as well as their subwavelength dimensions [4].

Recently, the underlying physics of an isolated SRR or CSRR and the interaction between SRRs or CSRRs and other elements, such as series interdigitated capacitive gaps [5] and electromagnetic bandgaps [6], have been deeply studied in planar technology leading to exotic electromagnetic behaviors such as left-handed propagation [4].

Corresponding author: M. Navarro-Cía (miguel.navarro@unavarra.es).

Among other consequences, EIWs are supported by CSRRs because of
the close interaction between neighbor elements [7, 8]. Therefore, in a
discontinuous microstrip that otherwise exhibits stop-band at certain
frequencies, a passband can be achieved at those frequencies if CSRRs
are etched on the ground plane, being propagation supported by the
existence of the CSRRs [7]. This approach is employed in this paper
in order to design coupled microstrip filters.

Subsequently, we further investigate the viability of coupling
microstrip lines within an enhanced ultra-wide bandwidth with filtering
response. The strategy used to improve the coupling bandwidth and
minimize the spurious bands arising at lower and higher frequencies
is to combine two electro-inductive coupling branches, i.e., two stages
in cascade. This leads to 70% measured bandwidth of the central
frequency and the spurious lower frequency lobe of -30 dB. Finally,
chains of CSRRs are designed to be placed underneath the access
microstrip lines in order to remove the undesired higher frequency
spurious band, taking advantage of the frequency selective nature of
the CSRR elements.

2. DESIGN AND FABRICATION OF THE ELECTRO-INDUCTIVE PARTICLE

A schematic with the relevant dimensions of the single-CSRR
configuration, as well as the fabricated prototypes, is presented in
Fig. 1. They consist of two microstrip lines with a separation between
line of $d_x = 1$ mm to each other and an overlap region $2d_z$. Within the
overlap area, that is, at the end of each microstrip, a CSRR is etched
on the ground plane. The relevant dimensions of the microstrip lines
and CSRRs are summarized in Table 1.

Table 1. Parameters of the single scheme (in mm).

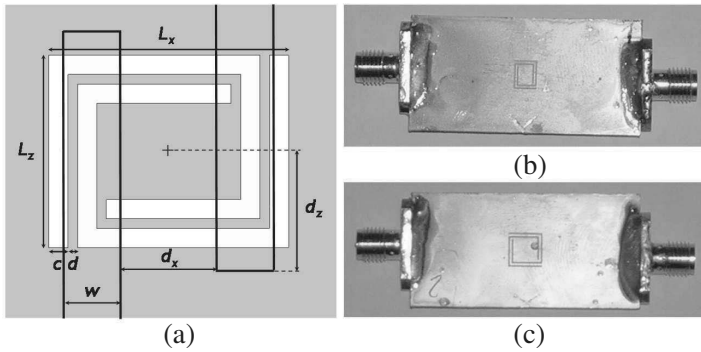| Parameters	Prototype 1	Prototype 2
L_x	5	6
L_z	4	6
w	1.2	1.2
c	0.5	0.3
d	0.1	0.3
d_x	1	1
d_z	2	3.25

Figure 1. (a) Schematic of the single topology with the relevant parameters. The microstrip lines are over-imposed to the CSRR. Bottom view of prototype 1 (b) and prototype 2 (c).
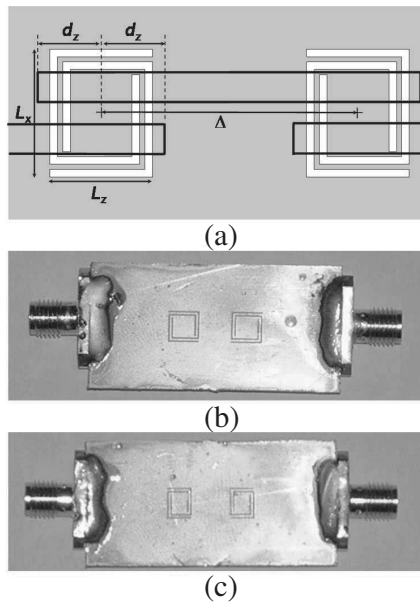

Figure 2. (a) Schematic of the double topology with the relevant parameters. Bottom view of prototype 1 (b) and prototype 2 (c).

On the other hand, the double topology, whose sketch and picture are shown in Fig. 2, presents three microstrip lines: one is split into two branches and adjacent to them at a distance $d_x = 0.8$ mm and 0.4 mm, for the first and second prototype respectively, a conductor strip which not only covers the gap region, but also overlaps slightly

Table 2. Parameters of the double scheme (in mm).

Parameters	Prototype 1	Prototype 2
L_x	5	5
L_z	4	5
Δ	10	10
w	1.2	1.2
c	0.3	0.3
d	0.2	0.2
d_x	0.4	0.8
d_z	2	3.5

with the two aforementioned branches. The CSRRs are etched on both ends of this central microstrip. The parameters regarding this double topology are presented in Table 2. Those not shown in Fig. 2(a) have the same meaning as before.

The substrate used for the design and fabrication was Rogers RO3010 with electrical permittivity $\varepsilon_r = 10.2$, height $h = 1.27\,\mathrm{mm}$, and conductor thickness $t = 0.035\,\mathrm{mm}$. The fabrication has been performed by a LPKF ProtoMat 93s numerical milling machine.

3. NUMERICAL AND EXPERIMENTAL RESULTS

Prior to the prototype fabrication, full wave simulation results have been obtained with the aid of the transient solver of the commercial software CST Microwave Studio^{TM}, which is based upon Finite Integration Time Domain Method. Let us start with the single-CSRR configuration and tackle the double topology subsequently.

Figure 3 shows the simulated S-parameters for the proposed designs without and with CSRR at their end for prototype 1 (Figs. 3(a) and 3(b)) and prototype 2 (Figs. 3(c) and 3(d)). As shown in the figure, the coupling between microstrip lines is negligible when the CSRR is not etched. However, when a CSRR is placed underneath the end of the microstrip lines, a clear passband from 3.5 GHz to 6.5 GHz for prototype 1 (Fig. 3(b)) and from 2.2 GHz to 4.4 GHz for prototype 2 (Fig. 3(d)) can be observed. Fig. 3 also reveals that at lower and higher frequencies, spurious bands appear. It is desirable to remove the spurious bands in a final prototype. This fact will be addressed afterwards.
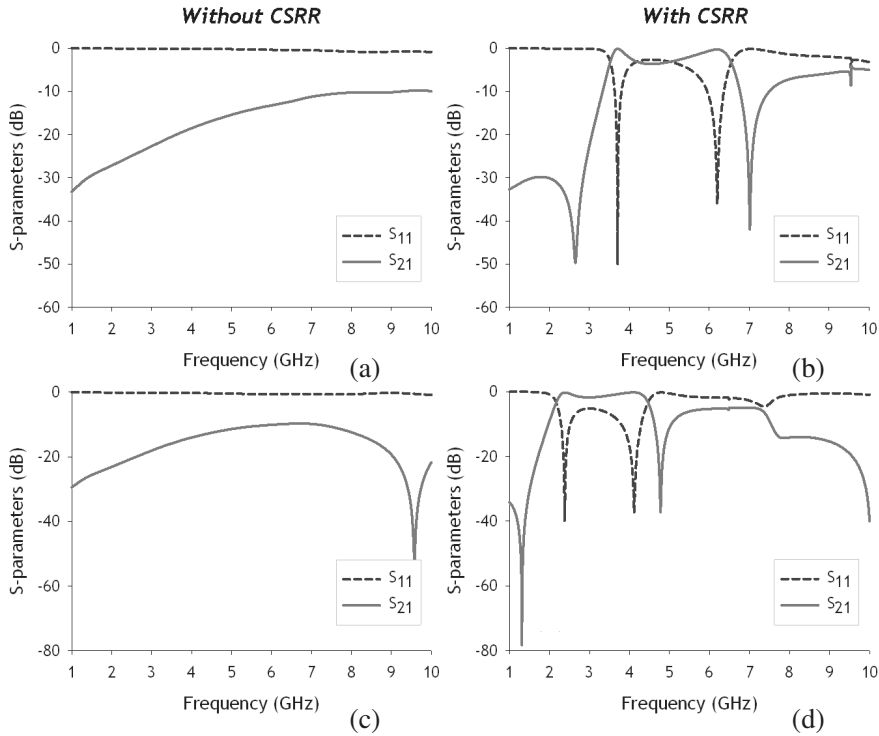
Figure 3. Simulated S-parameters (S_{11} and S_{21} are represented in dashed blue and solid red curves) for prototype 1 (b) and prototype 2 (d). Both prototypes without the etched CSRR are shown in (a) and (c) respectively, to stress the role of the EIW-based coupling through the CSRR.

Figure 4 shows the simulated S-parameters for the proposed double-scheme designs. Once again, in order to highlight the role of the EIWs (due to the etched CSRRs), the prototypes without and with CSRRs are rendered on the left- and right-hand sides respectively. The results display similar features to the single-scheme topologies: the inclusion of CSRRs gives rise (prototype 2, see Figs. 4(c) and 4(d)) or even broadens (prototype 1, see Figs. 4(a) and 4(b)) the coupling passband. It is worth noting in this case that compared with single CSRR configuration, the level of the spurious band at lower frequencies decreases to values below -45 dB in both cases. Therefore, the remaining concern is to remove the band observed at frequencies higher than 6 GHz.
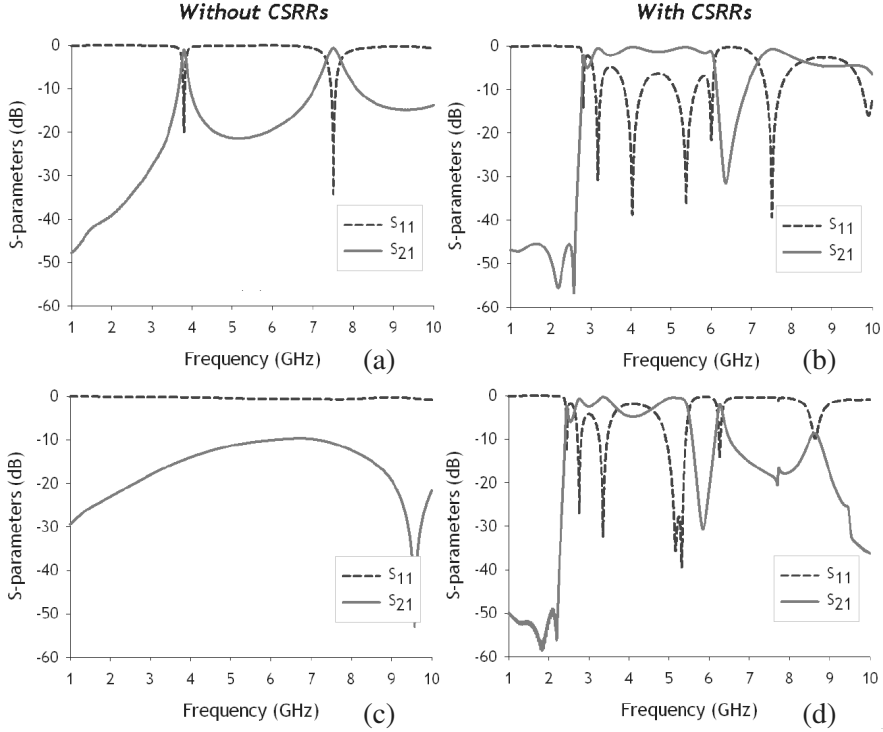
Figure 4. Simulated S-parameters (S_{11} and S_{21} are represented in dashed blue and solid red curves respectively) for double-scheme prototype 1 (b) and prototype 2 (d). Both prototypes without the etched CSRR are shown in (a) and (c) respectively, to stress the role of the EIW-based coupling through the CSRR.

To finish with the numerical analysis, we plot the average surface current at one random frequency within the passband (without loss of generality) for prototypes 1 of single- (Fig. 5(a)) and double-schemes (Fig. 5(b)). Notice that there is propagation along the whole planar transmission line, as it was expected from S-parameters, and an enhancement of the current density around the CSRRs on the ground plane (Notice that the average surface current is reduced at the sections of the microstrip lines above the CSRR). This reveals that the resonator is excited and supporting the EIW coupling.

Measurements have been carried out with an Agilent 8722ES VNA up to 10 GHz, using full two port 3.5 mm D connector calibration 3.5 mm. Figs. 6(a) and 6(b) show the S-parameters for the single-schemes, whereas Figs. 6(c) and 6(d) are given for the double-schemes.
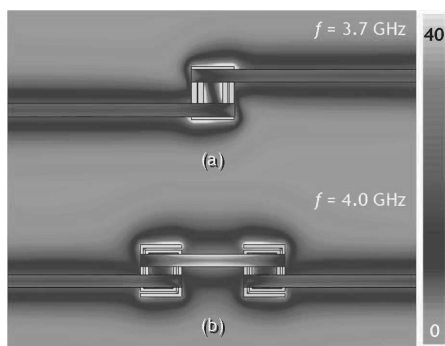
Figure 5. Average surface current (A/m) for prototypes 1 of single (a) and double topology (b).
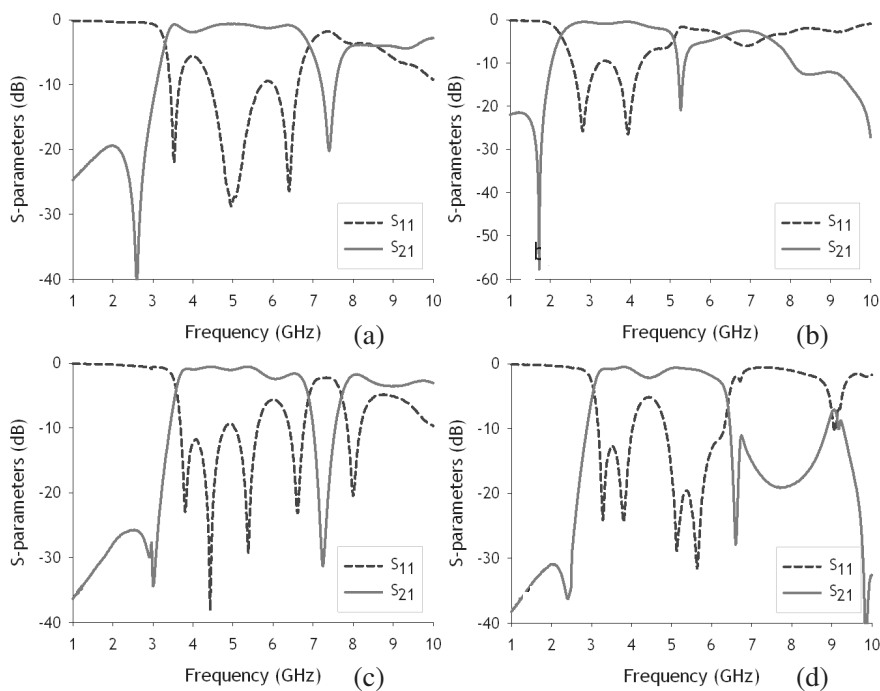

Figure 6. Measured S-parameters (S_{11} and S_{21} are represented in dashed blue and solid red curves respectively) for single-scheme (a) and (b), and double-scheme (c) and (d): prototype 1 (a), (c), and prototype 2 (b), (d).

As can be seen, there is good agreement between numerical and experimental results. In the case of single-scheme, the EIW passband extends experimentally from 3.3 GHz to 6.8 GHz for prototype 1 (Fig. 6(a)) and from 2.3 GHz to 5 GHz for prototype 2 (Fig. 6(b)), which implies a slight shift with respect to the simulation. Moreover, the passband suffers a lower ripple than predicted in simulations, which is a desired feature when one needs to fulfill specifications. The magnitude of the spurious bands is slightly higher than that in simulation due to tolerances in the fabrication process, slight changes in material parameters of the employed substrate batch and non-ideal behavior of the input/output connectors.

On the other hand, the EIW passband goes experimentally from 3.6 GHz to 6.8 GHz and from 3.0 GHz to 6.3 GHz for prototypes 1 and 2 of the double-scheme. In this case, the passband has been clearly reduced compared to the simulation, although the shape of the electromagnetic response is preserved. We are inclined to believe that this disagreement may be caused by some fabrication errors. Finally, the comments done in previous paragraph about the ripple within the passband and spurious bands can be brought about here as well.

4. ULTIMATE PROTOTYPE

It has been pointed out previously that it would be desirable to remove from the electromagnetic response the spurious bands that appear below and above the passband frequency range. The lower band has already been minimized by the double topology (two stages in cascade). Now, the approach to remove the higher band is to exploit the commonly used rejection response of the CSRR [4]. By placing a chain of tuned CSRRs underneath the access microstrip lines, one can design a wideband rejection band, which coincides with the undesired spurious band and thus, remove it [9]. Moreover, since the CSRR is operating in subwavelength regime, the occupied layout area by this chain of CSRRs is small.

The proposed design is rendered in Fig. 7(a). It is based on the prototype 2 of double-scheme together with a chain of CSRRs. The CSRRs have metal and air ring, as well as metal gap of 0.2 mm. The vertical dimension of the CSRRs is 2 mm, whereas the horizontal one ranges from 2.3 mm to 3.8 mm with a non-uniform step reached after an optimized procedure. The total length of the layout is 81 mm.

The simulated results can be seen in Fig. 7(b). As expected, the EIW passband remains present, and the first band appearing at around 6 to 8 GHz in preceding double-scheme prototypes has been removed clearly.
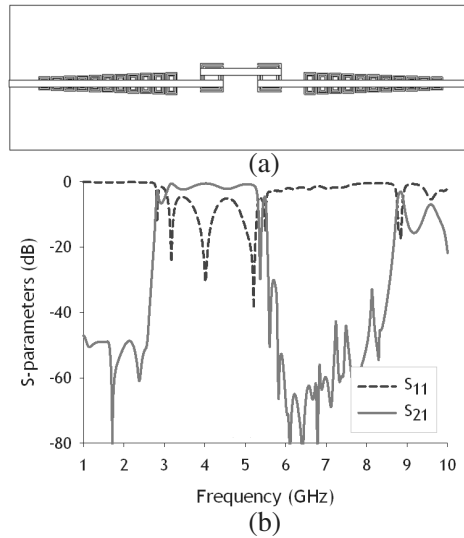
Figure 7. (a) Sketch of the proposed EIW-filter. (b) Simulated S-parameters (S_{11} and S_{21} are represented in dashed blue and solid red curves respectively).

5. CONCLUSION

In this paper, we show that electroinductive waves are a powerful tool to design wideband filters under the perspective of metamaterials, which may find application in devices such as image rejection filters, system diplexer and triplexer, antenna duplexer-filter and coupling circuits of several types. Despite the narrowband response commonly associated with split ring resonators and its complementary particle, by combining these resonators with discontinuous microstrip lines (note that capacitive-gaps have a long story in filters design, but their response is narrower than the one achieved by our prototype, which stresses the key role played by the CSRRs-based coupled filter), wideband responses are attainable as demonstrated in this work. Moreover, because of the subwavelength character of the CSRRs, the section providing the wideband coupling is clearly smaller than, for instance, coupled-line bandpass filters. Numerical results have been confirmed experimentally in the microwave regime.

ACKNOWLEDGMENT

REFERENCES

1. Solymar, L. and E. Shamonina, *Waves in Metamaterials*, Oxford University Press, New York, 2009.

2. Pendry, J. B., A. J. Holden, D. J. Robbins, and W. J. Stewart, "Magnetism from conductors and enhanced nonlinear phenomena," *IEEE Trans. Microw. Theory Tech.*, Vol. 47, No. 11, 2075–2084, 1999.

3. Falcone, F., T. Lopetegi, M. A. G. Laso, J. D. Baena, J. Bonache, M. Beruete, R. Marqués, F. Martín, and M. Sorolla, "Babinet principle applied to metasurface and metamaterial design," *Phys. Rev. Lett.*, Vol. 93, No. 12, 197491-1–197491-4, 2004.

4. Marqués, R., F. Martín, and M. Sorolla, *Metamaterials with Negative Parameters: Theory, Design, and Microwave Applications*, John Wiley and Sons, New York, 2008.

5. Jarauta, E., M. A. G. Laso, T. Lopetegi, F. Falcone, M. Beruete, J. D. Baena, J. Bonache, I. Gil, J. García-García, J. A. Marcotegui, F. Martín, R. Marqués, and M. Sorolla, "Novel microstrip backward coupler with metamaterial cells for fully planar fabrication techniques," *Microw. Opt. Tech. Lett.*, Vol. 48, No. 7, 1205–1209, 2006.

6. Navarro-Cía, M., F. Falcone, M. Beruete, I. Arnedo, J. Illescas, J. A. Marcotegui, M. A. G. Laso, and T. Lopetegi, "Left-handed behaviour in a microstrip line loaded with squared split-ring resonators and an EBG pattern," *Microw. Opt. Tech. Lett.*, Vol. 49, No. 11, 2689–2692, 2007.

7. Beruete, M., F. Falcone, M. J. Freire, R. Marqés, and J. D. Baena, "Electroinductive waves in chains of complementary metamaterial elements," *Appl. Phys. Lett.*, Vol. 88, No. 8, 083503-1–083503-3, 2006.

8. Navarro-Cía, M., M. Beruete, S. Agrafiotis, F. Falcone, M. Sorolla, and S. A. Maier, "Broadband spoof plasmons and subwavelength electromagnetic energy confinement on ultrathin metafilms," *Opt. Express*, Vol. 17, No. 20, 18184–18195, 2009.

9. Martin, F., F. Falcone, J. Bonache, R. Marqués, and M. Sorolla, "Miniaturized coplanar waveguide stop band filters based on multiple tuned split ring resonators," *IEEE Microw. Wirel. Comp. Lett.*, Vol. 13, No. 12, 511–513, 2003.